A DFT+U-D3 study of the adsorption of hydrogen fluoride and ethylene carbonate on the niobium-doped (001), (011), and (111) surfaces of lithium manganese oxide

Brian Ramogayana, [1, *] David Santos-Carballal, [2, **] Khomotso P. Maenetja, [1] Kemeridge T. Malatji[1], Nora H. de Leeuw[2, 3, †] and Phuti E. Ngoepe[1, ‡]

[1]*Materials Modelling Centre, School of Physical and Mineral Sciences, University of Limpopo, Private Bag x1106, Sovenga 0727, South Africa*
[2]*School of Chemistry, University of Leeds, Leeds LS2 9JT, United Kingdom*
[3]*Department of Earth Sciences, Utrecht University, Princetonlaan 8a, 3584 CB Utrecht, The Netherlands*

Abstract

Cationic doping has been recommended as one of the most effective methods of reducing the number of trivalent manganese (Mn^{3+}) ions that undergo a disproportionation reaction in lithium manganese oxide-based ($LiMn_2O_4$) lithium-ion batteries. However, the effect of surface doping on the major $LiMn_2O_4$ surfaces and their interactions with the electrolyte components is not yet fully understood. In this work, spin-polarised density functional theory-based calculations [DFT+*U*-D3 (BJ)] were employed to study the adsorption of the electrolyte components ethylene carbonate (EC) and hydrogen fluoride (HF) onto the Nb-doped major $LiMn_2O_4$ (001), (011), and (111) surfaces. During the substitution of niobium for manganese ions in the second surface layers (Nb_{second}), it was found that the (111) surface stability improves, resulting in an enhanced (111) plane on the morphology. However, replacing the first (Nb_{first}) as well as both top and sub-surface (Nb_{both}) layers of Mn atoms in the slabs maintains the same stability trend as in the pure pristine surfaces. Moreover, both adsorbates greatly preferred binding to the surfaces through the Nb instead of Mn atoms, and the largest adsorption energy was calculated for EC on the $LiMn_2O_4$ (011) surface doped on the Nb_{second} site and for HF on the $LiMn_2O_4$ (111) surface doped on the Nb_{both} site. Furthermore, the EC/HF adsorptions further enhance the stability of the Nb_{second} (111) surface plane. However, minimal charge transfer was calculated for both HF and EC interacting with the pure and Nb-doped surfaces. Our findings are interesting, since exposing the (111) surface promotes the formation of a stable solid electrolyte interface (SEI), significantly reducing Mn dissolution and enhancing the adsorption of EC and HF.

Keywords: ***Doping, adsorption, Density functional theory, Li-ion batteries, Surface chemistry***

* brianramogayana@gmail.com
** D.Santos-Carballal@leeds.ac.uk
† n.h.deleeuw@leeds.ac.uk
‡ phuti.ngoepe@ul.ac.za

Preprint submitted to Journal of the Electrochemical Society (JES) *26 August 2022*

1. Introduction

Lithium-ion battery (LIB) technology has gained significant traction as an alternative, clean, and renewable energy storage system that can facilitate a gradual movement away from the use of fossil fuels, and thus reduce the impact of global warming. Even though many studies have focused on developing other sustainable, earth-abundant, and low-cost alternative energy materials [1, 2, 3, 4], there is still no comparable replacement for LIBs. Rechargeable LIBs are widely applied in portable devices, electric vehicles, and stationary energy storage systems. However, the effective use of Li-ion batteries for large-scale applications is greatly influenced by the efficiency of the positive cathode materials [5, 6].

Among the materials explored [7, 8, 9, 10], the spinel lithium manganese oxide ($LiMn_2O_4$) has been reported as the most suitable and effective cathode material, owing to its low toxicity, affordability, high thermal stability, and high energy density [11, 12, 13, 14]. Most importantly, its three-dimensional crystal array allows a smooth reversible diffusion of Li^+ ions during cycling [15]. However, it experiences severe fading in capacity because of cathode-electrolyte interactions, which causes Mn^{2+} ion dissolution, Jahn-Teller distortion, and electrolyte oxidation, particularly at elevated temperatures [16, 17, 18, 19]. Fortunately, Jahn-Teller distortion and electrolyte oxidation can be controlled by cycling at restricted voltages [20, 21], although Mn dissolution remains a significant cause of deterioration.

Several techniques have been explored to suppress the Mn^{2+} ion dissolution and achieve high-capacity retention and improve electrochemical potential [22, 23, 24]. These strategies include the deposition of surface coating materials [25, 26, 27], surface/bulk doping [28, 29], the synthesis of spinel $LiMn_2O_4$ with exposed (111) facets, and tuned Mn^{3+} concentrations [30, 31]. Cation doping [32] in $LiMn_2O_4$ has been recommended as one the most effective methods to reduce the number of trivalent manganese (Mn^{3+}) ions that can undergo the disproportionation reaction outlined by Hunter [33], i.e.: $2Mn^{3+}_{(solid)} \rightarrow Mn^{4+}_{(solid)} + Mn^{2+}_{(solution)}$. Introducing dopants to replace Mn^{3+} thus limits the formation of Mn^{2+}, which are susceptible to dissolution. Many dopants, such as Al^{3+} [34, 35, 36], Co^{2+} [37], Ni^{2+} [38, 39, 40, 41], Ti^{4+} [42], Nb^{5+} [43, 44], Na^+ [45, 46, 47], F^- [48, 49], have been investigated previously and have shown improved structural stability and capacity retention in various cathode materials. Among these, Nb^{5+} was deemed one of the best dopants because of its stronger Nb-O binding energy compared to Mn-O [50]. Additionally, the ionic radius

of Nb^{5+} is comparable with that of Mn^{4+} and Li^{+} ions, which makes it possible to dope on either the lithium or transition metal (TM) sites [51].

Li et al [52], who studied the influence of Nb doping on the structure and electrochemical properties of $LiMn_2O_4$ spinel, found that doping using small amounts of Nb reduces the crystal volume and lattice parameters without affecting the Li^{+} transport. They also indicated that at different Nb contents, the diffraction peaks entirely belong to the spinel structure, even though small traces of $LiNbO_3$ impurities were found. Later, Li et al [53] discussed that Nb doping in spinel $LiMn_2O_4$ can improve the capacity and electrochemical performance and strengthen the crystal growth along the (111) and (400) planes. Other subsequent studies reported that similar to Cr doping, Nb doping improves Li diffusion in lithium manganese-based cathode materials [54, 55, 44, 43, 56].

However, doping the bulk spinel with atoms of different sizes and charges can yield different levels of cation order, leading to variations in capacity and cycling stability [57, 58]. Hence, surface doping is now considered the more effective method of stabilizing the spinel cathodes [59, 60, 61]. In this work, we employ the spin-polarized density functional theory calculations to study the effect of Nb doping on the major surfaces of the $LiMn_2O_4$ spinel material and their interactions with the electrolyte components, ethylene carbonate (EC) and hydrogen fluoride (HF). We discuss the effect of Nb doping on the first (Nb_{first}), second (Nb_{second}), and both first and second (Nb_{both}) layers, as well as the surface free energies, morphologies, and Bader charges. We also compare the single molecule adsorption of EC and HF onto the pristine and most stable Nb-doped configurations.

2. Computational methods

2.1. *Calculation details*

The Nb-doping and EC/HF adsorption at the major spinel surfaces were studied using the spin-polarized density functional theory (DFT) technique as implemented in the Vienna Ab initio Simulation Package (VASP) [62]. The calculations were carried out within the generalized gradient approximation (GGA) using the Perdew, Burke, and Ernzerhof (PBE) exchange-correlation functional [63]. For all the calculations, the kinetic energy cut-off was fixed at 560 eV, and a Γ-centered Monkhorst-Pack grid of 5×5×5 and 5×5×1 *k*-points was used for the bulk and

all the surfaces, respectively. Gaussian smearing with a width of 0.05 eV was included [64] to improve the convergence of the Brillouin zone integrations during geometry optimizations. The semi-empirical method of Grimme with the Becke-Johnson damping [D3-(BJ)] [65, 64] was included to model the long-range dispersion interactions and describe the surfaces properly [66, 67, 68, 69]. The projector augmented-wave (PAW) method [70] in the implementation of Kresse and Joubert [71] was used to describe the core electrons and their interaction with the valence electrons. A Hubbard correction [72] in the formulation of Dudarev and co-workers [73] was applied to improve the description of the localized 3*d* manganese electrons. From the range of values reported in the literature [74, 75, 76, 77] and consistent with our previous studies [41, 78, 79], we used the effective parameter, U_{eff} = 4.0 eV. The charge distributions were studied using the Bader scheme, implemented in the Henkelman code [80, 81, 82].

2.2. *Stability and adsorption energies calculations*

The stability of the lithium manganese oxide surfaces after incorporating niobium ($LiNb_xMn_{2-x}O_4$) and ethylene carbonate or hydrogen fluoride (EC/HF) adsorbates was evaluated by calculating their surface free energies (σ) using the equation:

$$\sigma = \gamma_r + \frac{E_{\text{doped}} - E_{\text{r}} - x \cdot E_{\text{Nb}} + x \cdot E_{\text{Mn}} - E_{\text{EC/HF}}}{A} \quad (1)$$

where E_{doped} is the energy of the $LiNb_xMn_{2-x}O_4$ doped surface, the $E_{\text{r,slab}}$ is the energy of the relaxed pristine surface, E_{EC} is the energy of the isolated EC/HF molecule, and E_{Nb} and E_{Mn} are the energies of one atom in the bulk of the body-centered cubic (*bcc*) niobium and manganese metal with the space group $Im\bar{3}m$ (No. 229), respectively. The geometry optimizations for isolated EC and HF molecules were carried out by sampling the Γ point of the Brillouin zone using a cell of 10 Å × 11 Å × 12 Å to avoid spurious interactions. For surfaces with no modifications (undoped and no adsorbates), the surface energies and surface free energies are the same, but a correction expression was added to account for modifications made. The resulting σ where then used to generate particle morphologies of the modified surfaces as compared to the pristine slabs. The morphologies were created using the GTK Display Interface for Structures (GDIS) program [83].

The adsorption energies of the EC/HF (E_{ads}) was calculated as the total energy difference of the adsorbed slab ($E_{EC/HF+slab}$) and the sum of the energies of the isolated EC/HF molecule, and the pure/doped surface, using the expression:

$$E_{ads} = E_{EC/HF+slab} - (E_{EC/HF} + E_{pure/doped}) \quad (2)$$

Positive adsorption energy indicates an endothermic process, while the negative values show an exothermic process.

To visualize the calculated charge transfer between the surfaces and the adsorbed molecules, we calculated the charge density difference ($\Delta\rho$). The $\Delta\rho$ was calculated as the sum of the electron charge densities of the pure/doped clean surface (ρ_{surf}), and an isolated EC/HF molecule ($\rho_{EC/HF}$), with identical structure as in the adsorbed form, deducted from the electron density of the total system comprising the surface and the adsorbed molecule (ρ_{sys}) as:

$$\Delta\rho = \rho_{sys} - (\rho_{surf} + \rho_{EC/HF}) \quad (3)$$

The charge density flow ($\Delta\rho$) and all other graphical structural drawings were created using the Visualization for Electronic and Structural Analysis (VESTA) program [84].

3. Results and discussions

3.1. Niobium doping and surface stability

To model the $LiMn_2O_4$ (001), (011), and (111) surfaces doped with Nb on the manganese positions, three doping scenarios were investigated and compared with the normal spinel surfaces modelled in our previous work *[79]*. The three possible scenarios considered were: (*i*) Nb atoms incorporated in the first (Nb_{first}), or (*ii*) second (Nb_{second}) layers, and (*iii*) in both the first and second (Nb_{both}) layers. In each scenario, various Mn positions were considered, as shown in Figure 1(*a-b*). There exist four {*i.e.* bridging, two hollow, and one corner} Mn positions on the Nb_{first} sites of the (001) surface while atop three and one Mn sites were considered for (011) and (111) surfaces, respectively. For Nb_{second}, several Mn sites were available, *i.e.* four, two, and six Mn positions in the (001), (011), and (111) surfaces, respectively. We explore small concentrations of Nb doping on the surfaces, *i.e.* $x = 0.125$ for Nb_{first} and Nb_{second}, and $x = 0.25$ for Nb_{both} (where two Nb atoms

were substituted at Mn positions of the first and second layers). Upon Nb substitution, the surface atoms were free to move and allowed to change their geometry.

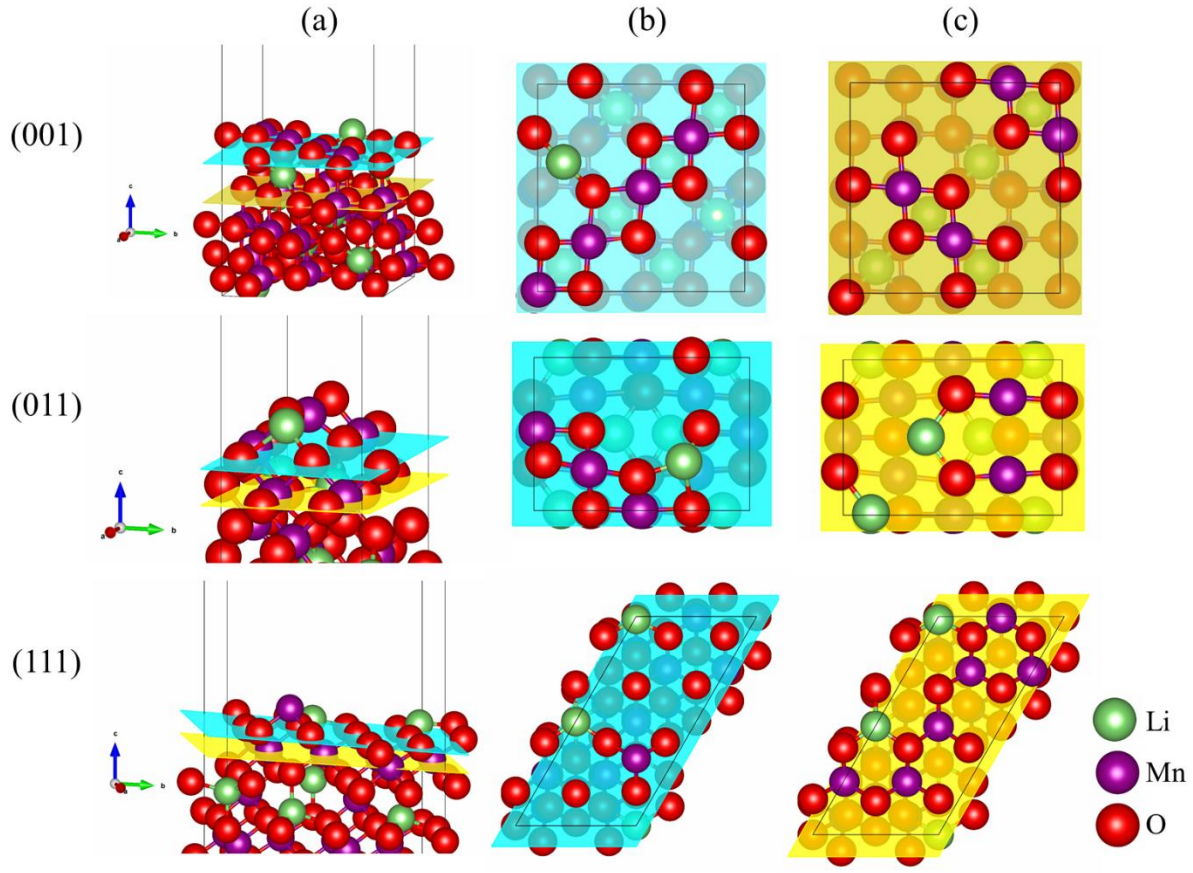

Figure 1: (a) Side and (b,c) top views showing the two top layers considered for niobium doping on the (001), (011), and (111) spinel $LiMn_2O_4$ surfaces. The first (Nb_{first}) and second (Nb_{second}) atomic layers are indicated in blue and yellow, respectively.

Figure 2 summarizes the calculated surface free energies (σ) for doping the Nb_{first}, $Nb_{second,}$ and Nb_{both} sites as compared to the surface energies previously calculated for the undoped spinel surfaces [79]. Upon doping, it was generally observed that the calculated σ increase as compared to the pure facets, suggesting that this process requires an energy input. For example, the σ increased from 0.037 to 0.210 $eV/Å^2$ after doping the Nb_{first} sites of the (001) surface with respect to the pristine facet, which was the smallest change observed. The incorporation of Nb on the Nb_{first} layer maintained the same stability trend as the pure pristine surfaces (*i.e.* (001) < (011) < (111)), but different results are obtained when doping the Nb_{second} and Nb_{both} sites. The surface free energies of the (011) facets are higher after doping on the Nb_{second} and Nb_{both} sites compared to the

pure (011) surface, resulting in a new stability trend, *i.e.* (001) < (111) < (011). As such, the (111) surface is stabilised for Nb_{second} and Nb_{both} doping, particularly the former case, even though the (001) remains the most stable facet.

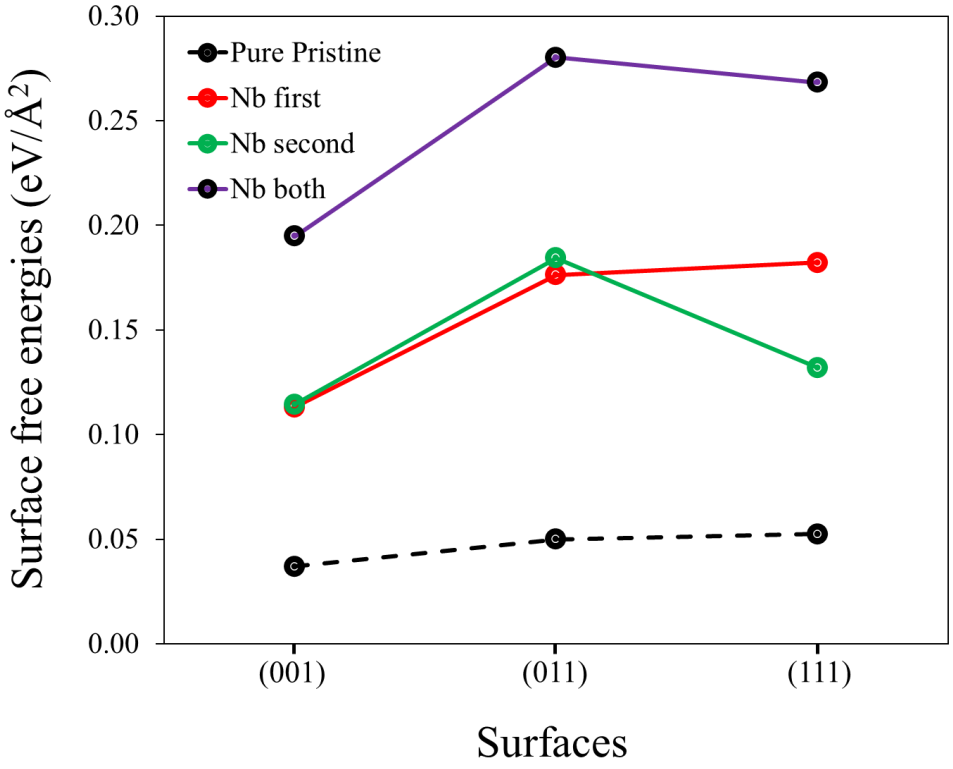

Figure 2: The calculated surface free energies of the facets with Nb substituted on different Mn positions, *i.e.* Nb_{first}, $Nb_{second,}$ and Nb_{both} as compared to the surface energies of pure pristine slabs.

3.2. Molecular adsorption

Here, we discuss the effect of the adsorption of the electrolyte components, ethylene carbonate (EC) and hydrogen fluoride (HF), on the niobium-doped $LiMn_2O_4$ surfaces as compared to the pure pristine facets. The binding sites considered include the bridging and hollow Mn/Nb sites for the (001) surface and on-top available Mn/Nb positions for the (011) and (111) surfaces, see Figure 3a. Initial EC interactions towards the surface was via the carbonyl (O_c) and the ethereal (O_e), oxygen atoms, while the HF was through the fluoride atom. The molecules were placed initially at 2.0 Å to favour the attractive forces between molecule and surface over the repulsive ones, although the atoms in the surfaces and the EC/HF were free to move and change their adsorption geometry upon relaxation. Referring to our previous work [79], the EC structural parameters were compared with the available experimental and theoretical data, which were in good agreement.

Similarly, the calculated internal bond distance for HF at d(H-F) = 0.937Å is in agreement with the available literature data of ~0.91 Å [85, 86, 87].

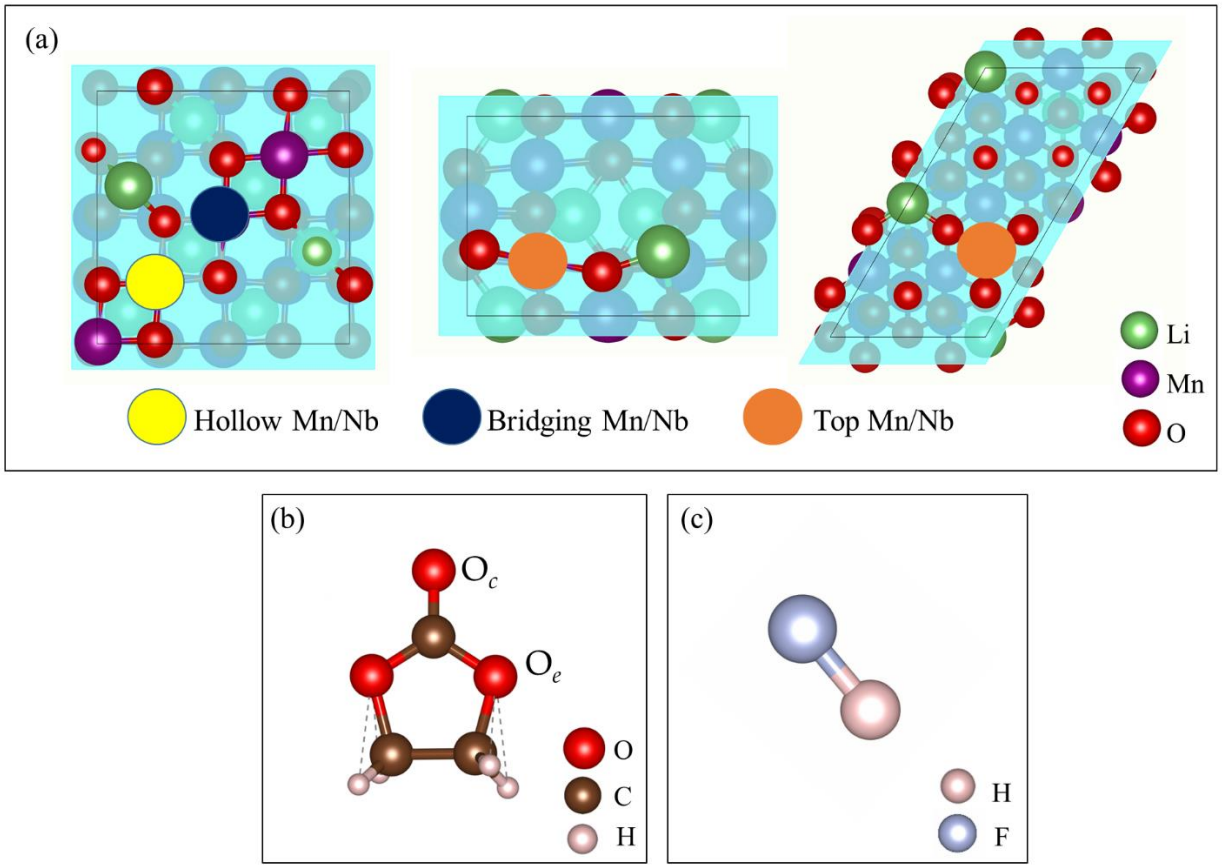

Figure 3: Schematic diagram showing the (a) adsorption Mn/Nb positions on the (001), (011) and (111) surfaces, (b) ethylene carbonate (EC) and (c) hydrogen fluoride (HF) molecules, indicating the carbonyl (O_c) and ethereal (O_e) oxygen.

3.2.1. *Ethylene carbonate adsorptions*

Figure 4 displays the structures and binding energies (E_{ads}) of the most stable interaction configurations of EC at the Nb-doped surfaces. The adsorption energies of EC at the Nb-doped surfaces were compared to those of the undoped surfaces. Various adsorption positions were explored, where the EC molecule was allowed to bind to the surfaces at the manganese or niobium atoms. After relaxation, the molecule preferred to bind to the surface through the Nb atoms rather than through the Mn, owing to the stronger Nb-O bond dissociation energy (~753 kJ/mol) compared to Mn-O (~402 kJ/mol) [88]. The EC molecule preferred binding on the surfaces when

placed parallel interacting with the slabs via the O_c. Generally, the largest adsorption energy was calculated for the Nb_{second} site of the (011) surface with E_{ads} = -5.13 eV at 2.25Å. For adsorptions on the surfaces with Nb atom, the EC molecule preferred to interact through the Nb instead of the Mn atom, and the most favoured configuration was on the $LiMn_2O_4$ (011) and (001) surface with Nb on the Nb_{first} and Nb_{both} site, respectively. Higher EC adsorption energies were generally observed for interactions with the Nb-doped surfaces compared to the pristine undoped surfaces [79].

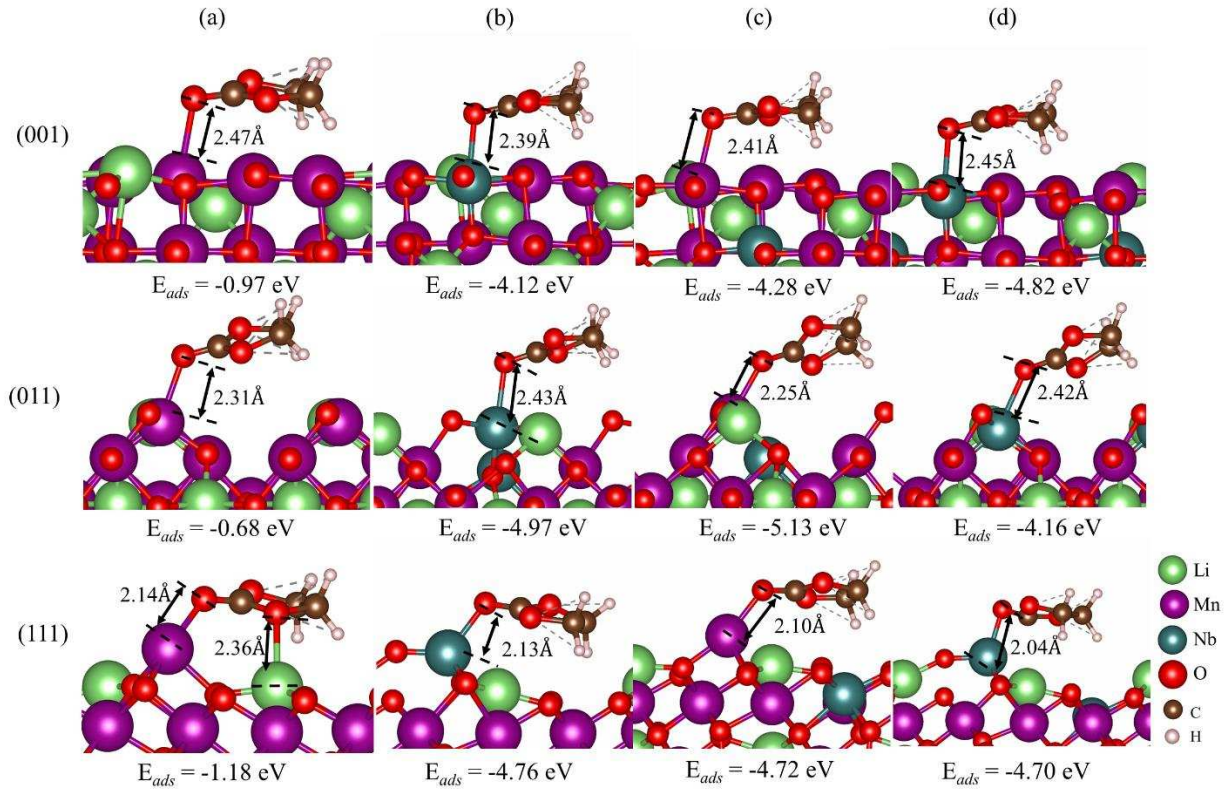

Figure 4: Adsorption energies and geometries calculated for ethylene carbonate (EC) molecule interacting with the Nb-doped spinel surfaces on the *(a) pure pristine, (b) first (Nb_{first}), (c) second (Nb_{second}),* and *(d) both (Nb_{both}) 1st and 2nd* atomic layers.

3.2.2. *Hydrogen fluoride adsorptions*

Figure 5 displays the interactions between the undoped and Nb-doped $LiMn_2O_4$ surfaces and the acidic component of the electrolyte, namely hydrogen fluoride (HF). Upon adsorption, the HF molecule was allowed to move and change geometry. As indicated in Figure 5, the HF molecule

relaxes and usually dissociates spontaneously to form Mn/Nb-F and O-H species, the latter also interacting with neighbouring surface oxygen via a hydrogen bonds (O-H···O). However, on the (001) surface both undoped and following doping on the Nb_{second} site, the HF molecule only interacts with the surfaces via a relatively weak hydrogen-bond, whereas it detaches from the Nb_{both} doped (111) surface. Generally, the highest binding energy was calculated for the Nb_{both} site of the (001) surface with E_{ads} = -5.66 eV. For pure undoped surfaces, HF molecule preferred to bind with the (111) surface, with E_{ads} = -4.26 eV. However, the adsorption of HF on the doped surfaces (*i.e.* Nb_{first}, Nb_{second} and Nb_{both} sites) generally released higher binding energies compared to the interaction with the stoichiometric surfaces.

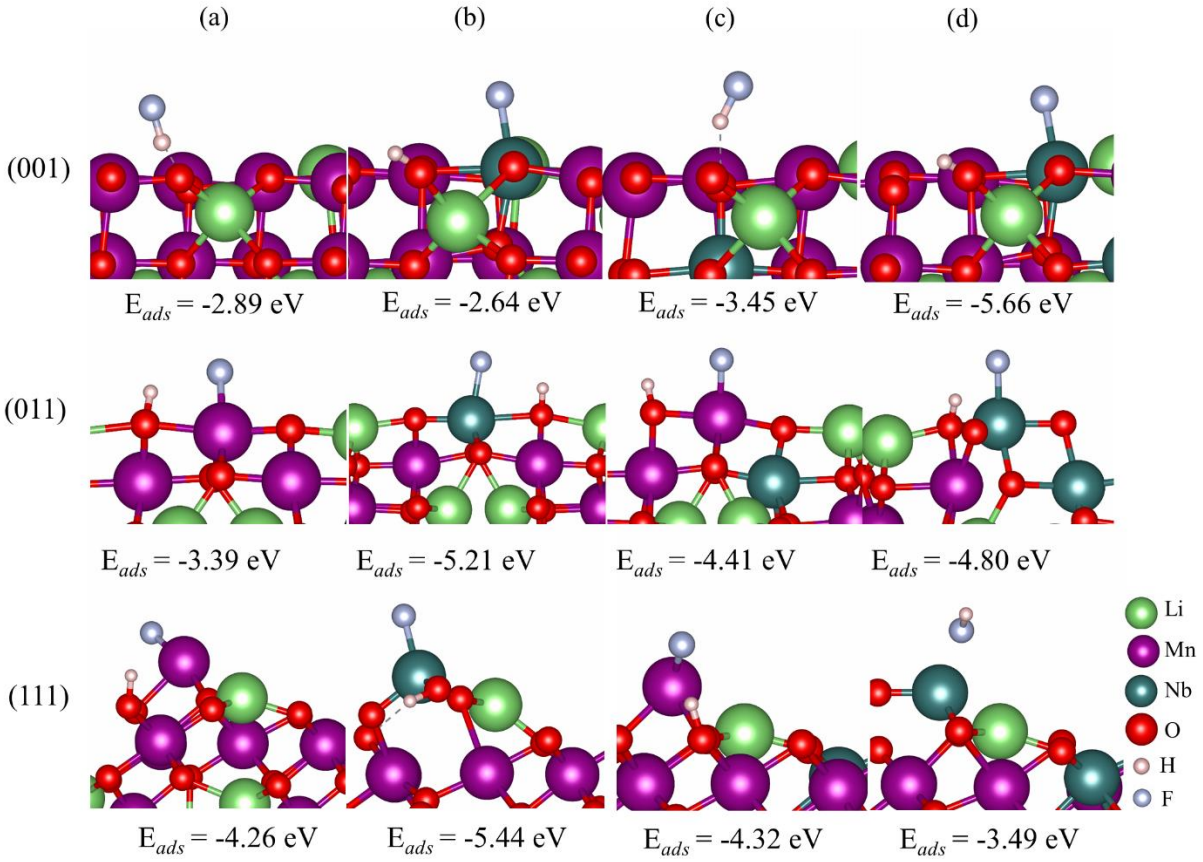

Figure 5: Adsorption energies and geometries calculated for hydrogen fluoride (HF) molecule interacting with the Nb-doped spinel surface on the *(a) pristine (b) first (Nb_{first}), (c) second (Nb_{second}),* and *(d) both (Nb_{both}) 1st and 2nd* atomic layers.

3.3. Morphologies

Next, we investigated the effect of Nb doping and adsorption of the electrolyte molecules on the nanoparticle morphologies, compared to the morphologies constructed for the undoped material. First, we discuss the effect of Nb doping on the surface morphologies, see Figure 6a, where we generally observe an enhancement of the (001) surface after doping the Nb_{first} site, and an increase in the expression of the (111) surface plane after doping the Nb_{second} and Nb_{both} positions, compared to the undoped surfaces. Nb doping in the second layers (Nb_{second}), in particular, stabilises and enhances the (111) plane, which is of significant interest, since it has been reported that this surface promotes the development of a stable solid electrolyte interface, which reduces Mn dissolution [89]. Secondly, we explored the effect on the morphologies of the adsorption of ethylene carbonate on the stable Nb-doped surfaces, see Figure 6b. From the constructed morphologies, it can be observed that upon adsorption of the EC molecule at the surfaces doped in the first (Nb_{first}) and both layers (Nb_{both}) sites, the (001) plane dominates the nanoparticles of the spinel. However, adsorption at the surface doped in the Nb_{second} site again causes dominance of the (111) plane. The (011) surface does not appear in the Wulff morphology upon doping alone, because of its higher surface free energy compared to the (001) and (111) planes. However, the (011) surface is expressed to a very minor degree after EC adsorption, but only for the Nb_{both} doped surfaces. Finally, we investigated the effect of HF adsorption on the stability of the pure and doped surfaces, see Figure 6c. The constructed morphologies for the undoped material indicate that the (111) surface dominates upon adsorption of HF. However, upon adsorption on the surfaces doped on the Nb_{second} site, the (111) plane increased in stability, dominating the morphology, while the (001) became prominent when the surfaces are doped in both the Nb_{first} and Nb_{both} sites.

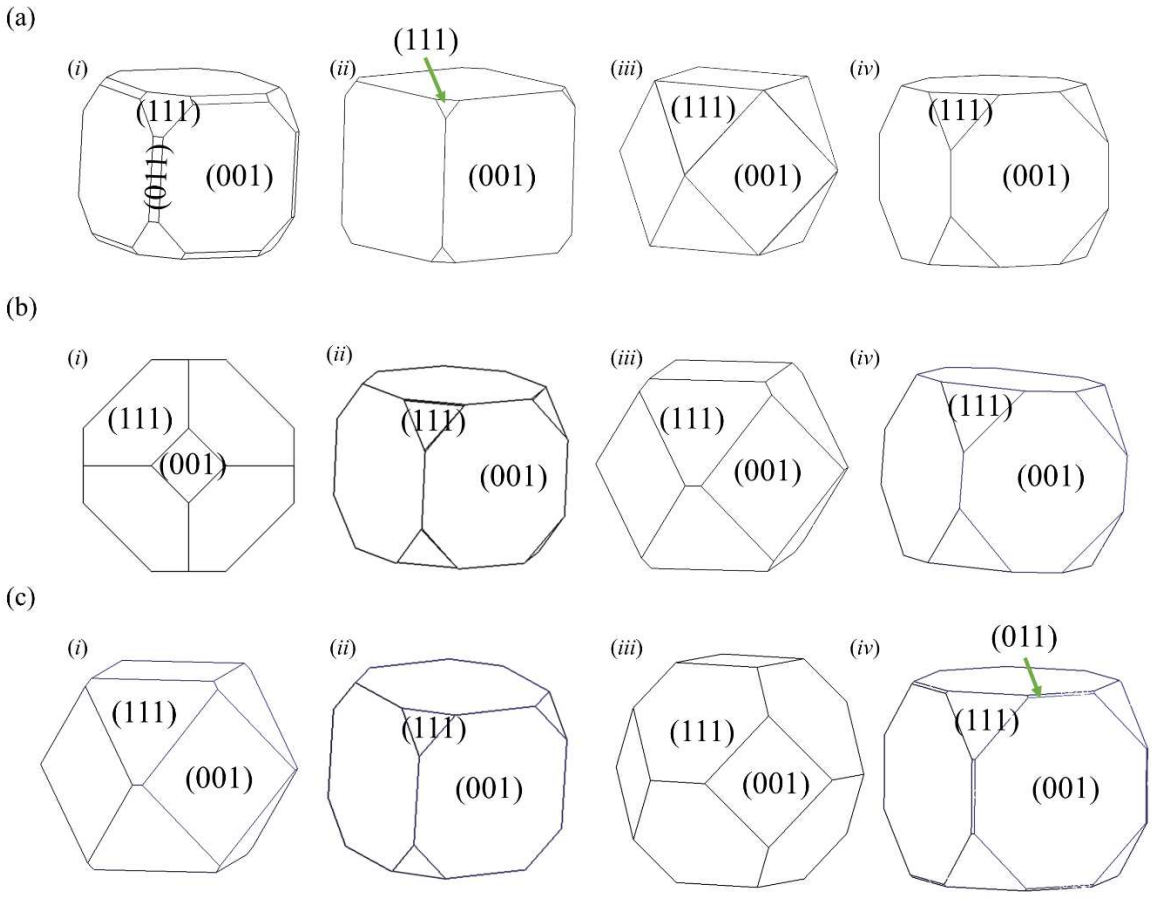

Figure 6. Constructed morphologies of the *(i)* undoped facets, and with Nb substituted on different Mn positions, *i.e.* (*ii*) Nb_{first}, (*iii*) Nb_{second} *and* (*iv*) Nb_{both}, for the (a) clean surfaces and with adsorbed (b) ethylene carbonate and (c) hydrogen fluoride.

3.4. Bader charge analysis

Table 1 summarizes the electronic charge transfer (Δq) analysis after EC/HF adsorption on the undoped and Nb-doped surfaces and their respective work functions (Φ). Generally, minimal charge transfer was observed between the adsorbed molecule (HF/EC) and the pure/Nb-doped surfaces. On the undoped surface, negligible charge transfers were calculated, with the highest values of -0.022 e^- observed for EC adsorbed on the (001) surface and -0.117 e^- for HF adsorbed on the (111) surface. For EC adsorbed on the Nb-doped surfaces, the highest charge transfers of -0.428 e^- was observed for the (111) surface doped on the Nb_{both} sites, with charge accumulation of 0.889 e^- on the surface. For HF adsorption, charge accumulation of 0.295 e^- was found on the Nb_{first}

doped (001) surface, with a charge depletion of 0.298 e^- and increase of -0.003 e^- on interacting F and H atoms, respectively. We also calculated and compared the charge difference between the interacting atom(s), *i.e.* carbonyl oxygen (O_c) in EC and H/F atoms, compared to the isolated adsorbate molecules ($\Delta q_{Oc/F}$ and Δq_H). For the EC molecule, partial oxidation and reduction were observed on the C and O atoms, respectively, which was caused by the intramolecular electron transfer from the C=O π-bond to an O-Mn/Nb σ-bond. We observed dissociation of the H-F bond, which resulted in the formation of new O-H and Nb/Mn-F bonds. Charge accumulation was observed on the H atom except on the Nb_{both} doped (001) surface.

Table I: Charge transfer between the EC and HF molecules and the surface (Δq) as well as the charge accumulation/depletion within the interacting atom and their respective work function (Φ). Negative charge transfer values indicate a charge accumulation on the adsorbate while positive values indicate charge transfers to the surface.

	Scenarios	Surface	Adsorption sites	$\Delta q_{EC/HF}$ (e^-)	$\Delta q_{Oc/F}$ (e^-)	Δq_H (e^-)	$\boldsymbol{\phi}$ (eV)
Ethylene carbonate (EC)	Undoped [79]	(001)		-0.022	0.810		3.453
		(011)		-0.004	0.800		4.446
		(111)		-0.005	0.784		3.545
	Nb_{first}	(001)	*Nb-Bridge*	0.008	0.799		4.214
		(011)	*Nb-Top*	-0.001	0.806		5.297
		(111)	*Nb-Top*	0.048	0.797		4.033
	Nb_{second}	(001)	*Mn-Hollow*	-0.016	0.802		4.073
		(011)	*Mn-Top*	0.009	0.804		5.056
		(111)	*Mn-Top*	0.001	0.773		3.669
	Nb_{both}	(001)	*Nb-Hollow*	-0.014	0.800		4.243
		(011)	*Top*	0.012	0.790		5.424
		(111)	*Top*	-0.428	0.889		3.869
Hydrogen fluoride (HF)	Undoped	(001)		-0.055	-0.044	-0.011	3.960
		(011)		-0.073	0.082	-0.155	4.903
		(111)		-0.117	-0.018	-0.099	4.354
	Nb_{first}	(001)	*Nb-Bridge*	0.295	0.298	-0.003	11.336
		(011)	*Nb-Top*	-0.079	0.073	-0.152	4.488
		(111)	*Nb-Top*	-0.011	0.110	-0.121	3.848
	Nb_{second}	(001)	*Mn-Hollow*	-0.056	-0.028	-0.028	3.838
		(011)	*Mn-Top*	-0.064	0.077	-0.141	5.017
		(111)	*Mn-Top*	-0.138	-0.008	-0.130	4.398
	Nb_{both}	(001)	*Nb-Hollow*	-0.086	-0.113	0.027	8.153
		(011)	*Top*	-0.069	0.088	-0.157	4.584
		(111)	*Top*	-0.165	-0.026	-0.140	3.425

We now compare the calculated work functions *(ϕ)* for the undoped and the Nb-doped surfaces after adsorption of the EC and HF molecules. The calculated ϕ for EC/HF surface interactions on the Nb-doped slabs as compared to pure pristine facets generally increase. This suggests that the reactivity EC/HF towards the surfaces upon Nb-doping reduces as compared to the pure undoped facets. Figure 7 summarises the charge density differences for the HF/EC adsorption configurations on the undoped and Nb-doped surfaces with the largest interface charge transfer. Despite the minor charge transfer observed after EC adsorptions, the electron flow plots show that the undoped surfaces suffered the largest charge rearrangement [79]. For the Nb-doped surfaces, we observe charge loss on the surface Nb atom and charge gain on the interacting atom of the adsorbate. We also observe significant charge rearrangements within the EC molecule as a result of the newly formed interfacial Nb-O σ-bond. For the HF adsorption, we found charge depletion and accumulation on the H and F atoms, respectively, upon the formation of the Mn/Nb-F and O-H σ-bonds between the surface and the adsorbates. We also observed partial charge accumulation and depletion on the neighbouring surface O atoms because of charge compensation effects with the Mn atom. Upon Nb doping, we also observed charge transfer within the O atoms of the subsurface layer.

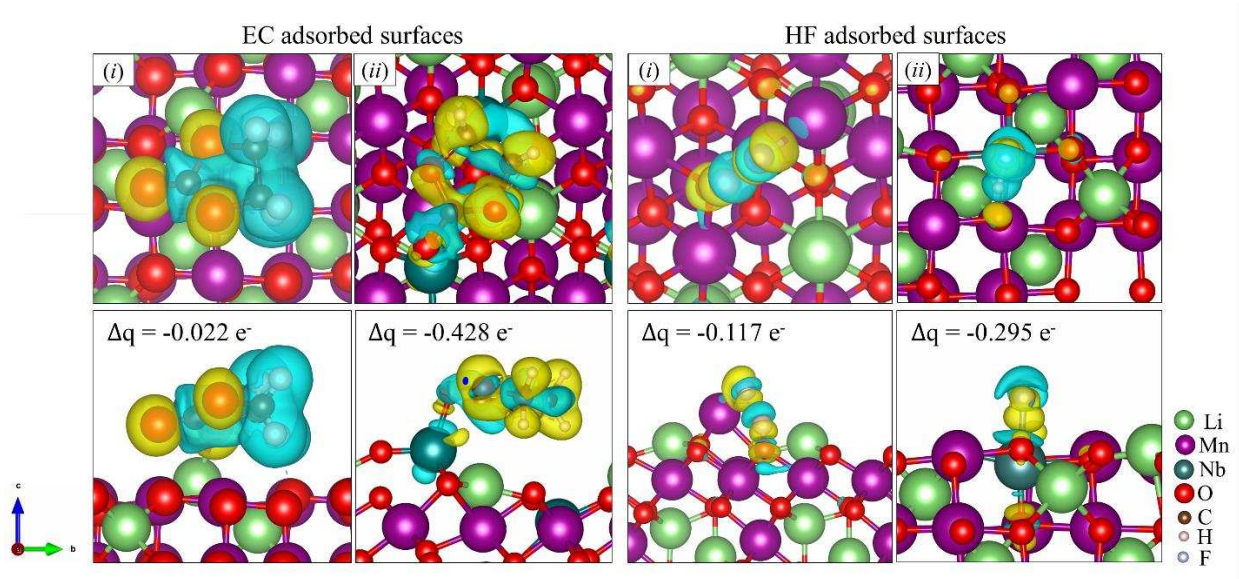

Figure 7: Top and side view of the charge density flow ($\Delta\rho$) for the adsorption configuration on the (*i*) pure and (*ii*) Nb-doped with the largest interface charge transfer. The density accumulation and depletion regions are indicated in yellow and blue, respectively. Isosurfaces display a value of

±0.012, ±0.010, ±0.008 and ±0.003 e/Å^3 for EC-pure, EC-Nb doped, HF-pure and HF-Nb doped $LiMn_2O_4$, respectively.

Conclusions

Spin-polarized density functional theory calculations have been employed to investigate the effect of Nb-doping on the major $LiMn_2O_4$ (001), (011) and (111) surfaces and their interactions with the electrolyte components, ethylene carbonate (EC) and hydrogen fluoride (HF). The calculated surface free energies of the Nb-doped facets increase compared to the surface energies of the undoped facets, indicating that this process requires high temperatures. Nb substitution in the second and both (*i.e.* Nb_{second} and Nb_{both}) layers greatly enhanced the dominance of the (111) surface plane in the Wulff morphology, whereas the same stability trend as in the pure surfaces is maintained when doping the first (Nb_{first}) layer. Interestingly, as exposing the (111) surface plane promotes the formation of stable solid electrolyte interfaces (SEI), which reduce Mn dissolution, we would suggest that Nb sub-surface doping would be a useful approach to obtain more (111) expression in the morphology.

Furthermore, the EC/HF electrolyte molecules greatly preferred binding to the surfaces through the Nb rather than Mn atoms, and the largest adsorption energy was calculated for EC on the Nb_{second}-doped (011) surface and for HF on the Nb_{both}-doped (111) surface. The adsorbates further enhance the expression of the (111) surface plane in the morphology, when they interact with the Nb_{second}-doped surfaces. The differential electron density indicates that EC adsorption on the surfaces is dominated by charge rearrangements within the molecule and partial accumulations/depletions on the interacting O atom as a result of the formation of interfacial Nb-O σ-bonds. Charge loss and gain was also observed on the H and F atoms interacting with the Mn/Nb and O atoms, respectively. Moreover, the calculated work function for EC/HF surface interactions on the Nb-doped slabs as compared to pure pristine facets generally increase, suggesting that the reactivity of electrolyte components towards the surfaces reduces upon niobium doping. In future work, we aim to explore and understand the kinetics and thermodynamic decomposition of the electrolyte components on the modified surfaces during charge/discharge.

Acknowledgments

The authors acknowledge funding from the UK Economic and Social Research Council (ESRC grant no. ES/N013867/1) and the National Research Foundation South Africa for funding of a UK-SA Newton Ph.D. partnership programme. PEN acknowledges the financial support of the DSI-NRF South African Research Chair Initiative and NHdL acknowledges the UK Engineering and Physical Sciences Research Council (EPSRC grant EP/K009567) for funding. We acknowledge the use of the Centre for High-Performance Computing (CHPC) facility of South Africa in the completion of this work. We also appreciate the support received from DSI Energy Storage Research Development and Innovation Initiative, South Africa. This work was performed using the computational facilities of the Material Modelling Centre (MMC), University of Limpopo, the Centre for High-Performance Computing, in Cape Town, and the Supercomputing Facilities at Cardiff University operated by ARCCA on behalf of the HPC Wales and Supercomputing Wales (SCW) projects. All data created during this research are presented in this paper.

Conflicts of interest

There are no conflicts to declare.

Authors Information

a. **Brian Ramogayana** – *Email*: brianramogayana@gmail.com, ORCID: https://orcid.org/0000-0001-6912-1597

b. **David Santos-Carballal -** *Email*: D.Santos-Carballal@leeds.ac.uk, ORCID: https://orcid.org/0000-0002-3199-9588

c. **Khomotso P. Maenetja -** *Email:* khomotso.maenetja@ul.ac.za, ORCID: https://orcid.org/0000-0002-3199-0946

d. **Kemeridge T. Malatji** – *Email:* kemeridge.malatji@ul.ac.za, ORCID: https://orcid.org/0000-0001-9071-854X

e. **Nora De Leeuw -** *Email*: n.h.deleeuw@leeds.ac.uk, ORCID: https://orcid.org/0000-0002-8271-0545

f. **Phuti E. Ngoepe** - *Email*: phuti.ngoepe@ul.ac.za, ORCID: https://orcid.org/0000-0003-0523-5602

References

[1] B. Fan, D. Zhang, M. Li, W. Zhong, Z. Zeng, L. Ying, F. Huang and Y. Cao, *Sci. China Chem.,* **62**, 746-752 (2019).

[2] B. Abdullah, S.A.F.A.S. Muhammad, Z. Shokravi, S. Ismail, K.A. Kassim, A.N. Mahmood and M.M.A. Aziz, *Renew. Sustain. Energy Rev.,* **107**, 37-50 (2019).

[3] E. Fan, L. Li, Z. Wang, J. Lin, Y. Huang, Y. Yao, R. Chen and F. Wu, *Chem. Rev.,* **120**, 7020-7063 (2020).

[4] Q.T. Phan, K.C. Poon and H. Sato, *Int. J. Hydrog. Energy,* **46**, 14190 - 14211 (2021).
[5] V. Mathew, B. Sambandam, S. Kim, S. Kim, S. Park, S., Lee, J. Lee, S. Park, J. Song and J. Kim, *J. Power Sources,* **472**, 228368 (2020).
[6] Y. Chen, K. Xie, C. Zheng, Z. Ma and Z. Chen, *ACS Appl. Mater. Interfaces,* 6, 16888 - 16894 (2014).
[7] P. Byeon, H.B. Bae, H.S. Chung, S.G. Lee, J.G. Kim, H.J. Lee, J.W. Choi and S.Y. Chung, *Adv. Funct. Mater.,* **28**, 1804564 (2018).
[8] K. Ozawa, *Solid State Ionics,* **69**, 212 - 221 (1994).
[9] D.W. Han, S.J. Lim, Y.I Kim, S.H. Kang, Y.C. Lee and Y.M. Kang, *Chem. Mater.,* **26**, 3644 - 3650 (2014).
[10] T. Mueller, G. Hautier, A. Jain and G. Ceder, *Chem. Mater.,* **23**, 3854 - 3862, (2011).
[11] M.M. Thackeray and K. Amine, *Nat. Energy ,* vol. 6, p. 566, 2021.
[12] W. Tang, Y. Hou, F. Wang, L. Liu, Y. Wu and K. Zhu, *Nano lett.,* **13**, 2036 - 2040 (2013).
[13] C.Y. Ouyang, S.Q. Shi, Z.X. Wang, H. Li, X.J Huang and L.Q. Chen, *Europhysics Lett.,* **67**, 28 (2004).
[14] R.S. Ledwaba, M.G. Matshaba and P.E. Ngoepe, *IOP Conf. Ser.: Mater. Sci. Eng.,* **80**, 012024-1 - 012024-5 (2015).
[15] J.C. Hunter, *J. Solid State Chem.,* **39**, 142-147 (1981).
[16] P. Arora, R.E. White and M. Doyle, *J. Electrochem. Soc.,* **145**, 3647 – 3667 (1998).
[17] Y. Dai, L. Cai and R.E. White, *J. Electrochem. Soc.,* **160**, A182 - A190 (2013).
[18] N.S. Choi, J.G. Han, S.Y. Ha, I. Park and C.K. Back, *RSC Adv.,* **5**, 2732 - 2748 (2015).
[19] X. Sun, R. Xiao, X. Yu and H. Li, *Langmuir,* **37**, 5252 - 5259 (2021).
[20] Y. Xia, Y. Zhou and M. Yoshio, *J. Electrochem. Soc.,* **144**, 2593 - 2600 (1997).
[21] K.L. Bassett, R.E. Warburton, S. Deshpande, T.T. Fister, K. Ta, J.L. Esbenshade, A. Kinaci, M.K. Chan, K.M. Wiaderek, K.W. Chapman and J.P. Greeley, *Adv. Mater. Interfaces,* **6**, 1801923 (2019).
[22] G. Xu, Z. Liu, C. Zhang, G. Cui and L. Chen, *J. Mater. Chem. A,* **3**, 4092 - 4123 (2015).
[23] T.R. Somo, T.E. Mabokela, D.M. Teffu, T.K. Sekgobela, B. Ramogayana, M.J. Hato and K.D. Modibane, *Coatings, **11**, 744. (*2021).
[24] C. Cai and G.M. Koenig Jr, *Electrochim. Acta, **401**, 139484. (*2022).
[25] C. Li, H.P. Zhang, L.J. Fu, H. Liu, Y.P. Wu, E. Rahm, R. Holze and H.Q. Wu, *Electrochimi. Acta,* **51**, 3872 - 3883 (2006).
[26] D. Zuo, G. Tian, X. Li, D. Chen and K. Shu, *J. Alloys Compd.,* **706**, 24 - 40 (2017).
[27] B. Ramogayana, D. Santos-Carballal, K.P. Maenetja, N.H. de Leeuw and P.E. Ngoepe, *ACS omega,* **6**, 29577 – 29587 (2021).
[28] Q. Liu, S. Wang, H. Tan, Z. Yang and J. Zeng, *Energies,* **6**, 1718 - 1730 (2013).
[29] W. Yan, S. Yang, Y. Huang, Y. Yang and G. Yuan , *J. Alloys Compd.,* **819**, 153048 (2020).
[30] F.P. Nkosi, C.J. Jafta, M. Kebede, L. Le Roux, M.K. Mathe and K.I. Ozoemena, *RSC Adv.,* **5**, 32256 - 32262 (2015).
[31] K. Raju, F.P. Nkosi, E. Viswanathan, M.K. Mathe, K. Damodaran and K.I. Ozoemena, *Phys. Chem. Chem. Phys.,* **18**, 13074 - 13083 (2016).
[32] Y. Huang, Y. Dong, S. Li, J. Lee, C. Wang, Z. Zhu, W. Xue, Y. Li and J. Li, *Adv. Energy Mater.,* **11**, 2000997 (2021).
[33] J.C. Hunter, *J. Solid State Chem.,* **39**, 142 – 147 (1981).

[34] Z. Cai, Y. Ma, X. Huang, X. Yan, Z. Yu, S. Zhang, G. Song, Y. Xu, C. Wen and W. Yang, *J. Energy Storage,* **27**, 101036 (2020).
[35] Y.L. Ding, J. Xie, G.S. Cao, T.J. Zhu, H.M. Yu and X.B. Zhao, *J. Phys. Chem. C,* **115**, 9821 - 9825 (2011).
[36] M. Chen, R. Wu, S. Ju, X. Zhang, F. Xue and W. Xing, *Microporous Mesoporous Mater., **261**,* 29 - 34 (2018).
[37] D. Xu, F. Yang, Z. Liu, X. Zeng, Y. Deng, Y. Zheng, H. Lou and S. Liao, *Ionics,* **26**, 3777-3783 (2020).
[38] D. Narsimulu, E.S. Srinadhu and N. Satyanarayana, *Ionics,* **3**, 981 - 990 (2018).
[39] A. Iqbal, A.M. Khan, T. Wang, D. Li and Y. Gao, *Int. J. Electrochem. Sci.,* **14**, 929 - 942 (2019).
[40] W. Liu, H. Xu, Q. Zhou, Y. Dai, W. Hu and H. Li, *J. Electron. Mater,* **49**, 5523 - 5527 (2020).
[41] K.T. Malatji, D. Santos-Carballal, U. Terranova, P.E. Ngoepe and N.H. de Leeuw, *S. Afr. J. Chem.,* **74**, 3 - 7 (2021).
[42] B. Zong, Y. Lang, S. Yan, Z. Deng, J. Gong, J. Guo, L. Wang and G. Liang, *Mater. Today Commun.,* **24**, 101003 (2020).
[43] S. Zheng, A. Dou, M. Su and Y. Liu, *Nanosci. Nanotechnol.,* **20**, 452-459 (2020).
[44] S. Zhang, W. Deng, R. Momen, S. Yin, J. Chen, A. Massoudi, G. Zou, H. Hou, W. Deng and X. Ji, *J. Mater. Chem. A,* **9**, 21532 - 21550 (2021).
[45] F. Sun and Y. Xu, *J. Alloys and Compd.,* **584**, 538-541 (2014).
[46] Y. Liu, D. Liu, H.H. Wu, X. Fan, A. Dou, Q. Zhang and M. Su, *ACS Sustain. Chem. Eng.,* **6**, 13045-13055 (2018).
[47] P. Zhang, X. Zhai, H. Huang, J. Zhou, X. Li, Y. He and Z. Guo, *Electrochim. Acta,* **349**, 136402 (2020).
[48] Y. Wang, H.T. Gu, J.H. Song, Z.H. Feng, X.B. Zhou, Y.N. Zhou, K. Wang and J.Y. Xie, *J. Phys. Chem. C,* **122**, 27836-27842 (2018).
[49] L. Fang, M. Wang, Q. Zhou, H. Xu, W. Hu and H. Li, *Colloids Surf. A Physicochem. Eng. Asp.,* **600**, 124940 (2020).
[50] S. Liu, Z. Liu, X. Shen, W. Li, Y. Gao, M.N. Banis, M. Li, K. Chen, L. Zhu, R. Yu and Z. Wang, *Adv. Energy Mater.,* **8**, 1802105 (2018).
[51] J. Ma, Y.N. Zhou, Y. Gao, Q. Kong, Z. Wang, X.Q. Yang and L. Chen, *Eur. J. Chem.,* **20**, 8723 - 8730 (2014).
[52] J. Li, Y. Tian and C. Xu, *J Mater. Sci. Technol.,* **28**, 817 - 822 (2012).
[53] W. Li, G.W. Siqin, Z. Zhu, L. Qi and W.H. Tian, *Chin. Chem. Lett.,* **28**, 1438 - 1446 (2017).
[54] Y. Lei, J. Ai, S. Yang, C. Lai and Q. Xu, *J. Taiwan Inst. Chem. Eng.,* **97**, 255 - 263 (2019).
[55] J. Wu, H. Liu, X. Ye, J. Xia, Y. Lu, C. Lin and X. Yu, *J. Alloys Compd.,* **644**, 223 - 227 (2015).
[56] J. Mao, K. Dai, M. Xuan, G. Shao, R. Qiao, W. Yang, V.S. Battaglia and G. Liu, *ACS Appl. Mater. Interfaces,* **8**, 9116 - 9124 (2016).
[57] R. Santhanam and B. Rambabu, *J. Power Sources,* **195**, 5442 - 5451, (2010).
[58] J. Yang, X. Han, X. Zhang, F. Cheng and J. Chen, *Nano Res.,* **6**, 679 - 687 (2013).
[59] J. Lu, C. Zhan, T. Wu, J. Wen, Y. Lei, A.J. Kropf, H. Wu, D.J. Miller, J.W. Elam, Y.K. Sun and X. Qiu, *Nat. Commun.,* **5**, 1 - 8 (2014).

[60] J.Y. Piao, Y.G. Sun, S.Y. Duan, A.M. Cao, X.L. Wang, R.J. Xiao, X.Q. Yu, Y. Gong, L Gu, Y. Li and Z.J. Liu, *Chem.,* **4**, 1685-1695 (2018).
[61] Y. Xue, L.L. Zheng, J. Wang, J.G. Zhou, F.D. Yu, G.J. Zhou and Z.B. Wang, *ACS Appl. Energy Mater.,* **2**, 2982 - 2989 (2019).
[62] G. Kresse and J. Furthmüller, *Phys. Rev. B,* **54**, 11169 (1996).
[63] J.P. Perdew, K. Burke and M. Ernzerhof, *Phys. Rev. Lett.,* **77**, 11169 - 11186 (1996).
[64] S. Grimme, J. Antony, S. Ehrlich and H. Krieg, *Chem. Phys.,* **132**, 154104 (2010).
[65] S. Grimme, S. Ehrlich and L. Goerigk, *J. Comput. Chem.,* **32**, 1456 - 1465 (2011).
[66] D. Santos-Carballal, A. Roldan, R. Grau-Crespo and N.H. de Leeuw, *Phys. Chem. Chem. Phys.,* **16**, 21082 - 21097 (2014).
[67] D. Santos-Carballal, A. Roldan and N.H. de Leeuw, *J. Phys. Chem.,* **120**, 8616 – 8629 (2016).
[68] D. Santos-Carballal, A. Roldan, N.Y. Dzade and N.H. de Leeuw, *Philos. Trans., Math. Phys. Eng. Sci.,* **376**, 20170065 (2018).
[69] V. Postica, A. Vahl, J. Strobel, D. Santos-Carballal, O. Lupan, A. Cadi-Essadek, N.H. de Leeuw, F. Schütt, O. Polonskyi, T. Strunskus, M. Baum, L. Kienle, R. Adelung and F. Faupel, *J. Mater. Chem. A,* **6**, 23669 - 23682, (2018).
[70] P. Blöchl, *Phys. Rev. B,* **50**, 17953 - 17979 (1994).
[71] G. Kresse and D. Joubert, *Phys. Rev. B,* **19**, 1758 - 1775 (1999).
[72] V.I. Anisimov, M.A. Korotin, J. Zaanen and O.K. Andersen, *Phys. Rev. Lett.,* **68**, 345 - 348 (1992).
[73] S.L. Dudarev, G.A Botton, S.Y. Savrasov, C.J. Humphreys and A.P. Sutton, *Phys. Rev. B,* **57**, 1505 – 1509 (1998).
[74] C.Y. Ouyang, S.Q. Shi and M.S. Lei, *J. Alloys Compd.,* **474**, 370 - 374 (2009).
[75] J. Bhattacharya and C. Wolverton, *Phys. Chem. Chem. Phys.,* **15**, 6486 - 6498 (2013).
[76] A. Karim, S. Fosse and K.A. Persson, *Phys. Rev. B,* **87**, 075322 (2013).
[77] C.Y. Ouyang, X.M. Zeng, Z. Sljivancanin and A. Baldereschi, *J. Phys. Chem. C,* **114**, 4756 - 4759 (2010).
[78] D. Santos-Carballal, P.E. Ngoepe and N.H. de Leeuw, *Phys. Rev. B,* **97**, 085126 (2018).
[79] B. Ramogayana, D. Santos-Carballal, P.A. Aparicio, M.G. Quesne, K.P. Maenetja, P.E. Ngoepe, and N.H. de Leeuw, *Phys. Chem. Chem. Phys.,* **22**, 6763 – 6771 (2020).
[80] M. Yu and D.R. Trinkle, *J. Chem. Phys.,* **134**, 064111 (2011).
[81] E. Sanville, S.D. Kenny, R. Smith and G. Henkelman, *J. Comput. Chem.,* **28**, no. 5, pp. 899 - 908 (2007).
[82] W. Tang, E. Sanville and G. Henkelman, *J. Condens. Matter Phys.,* **21**, 084204 (2009).
[83] S. Fleming and A. Rohl, *Z. Kristallogr. Cryst. Mater,* **220**, 580 - 584 (2005).
[84] V. Wang, N. Xu, J.C. Liu, G. Tang and W.T. Geng, *arXiv preprint arXiv:1908.08269, (*2019).
[85] C. Lee, C. Sosa, M. Planas and J.J. Novoa, *J. Chem. Phys.,* **104**, 7081 - 7085 (1996).
[86] E.M. Cabaleiro-Lago, J.M. Hermida-Ramón and J. Rodríguez-Otero, *J. Chem. Phys.,* **117**, 3160-3168 (2002).
[87] S. Odde, B.J. Mhin, H.M. Lee and K.S. Kim , *J. Chem. Phys.,* **121**, 11083-11087 (2004).
[88] Z. Yang, W. Xiang, Z. Wu, F. He, J. Zhang, Y. Xiao, B. Zhong and X. Guo, *Ceram. Int.,***43**, 3866 - 3872 (2017).
[89] M. Hirayama, H. Ido, K. Kim, W. Cho, K. Tamura, J.I. Mizuki and R. Kanno, *J. Am. Chem. Soc.,* **132**, 15268 - 15276 (2010).